Experimental determination of momentum resolution in DIRAC using Lambda events

B. Adeva, A. Romero, O. Vázquez Doce

University of Santiago de Compostela, Spain

Abstract

This note describes a method to determine the momentum resolution δp of DIRAC spectrometer, using only experimental data. The momentum dependence of $\delta p/p$ is parametrised with two coefficients, which are accurately determined for Ni 2001 data, using lambda events at low decay angle. Independently, an assesment of the experimental error in $\pi^+\pi^-$ opening angle is done, using the measured distance between track extrapolations to the target plane, for prompt pairs. As a result from both studies, a Monte Carlo simulation is constructed where resolution in longitudinal (Q_L) and transvers (Q_T)compoments of Q exactly matches the experimental data.

DIRAC internal note 2004-06 *30 July 2004*

1 Introduction

In the DIRAC experiment, the detection of pionium signal over the background Coulomb pairs relies directly on having a sufficiently good momentum resolution in the $\pi^+\pi^-$ center-of-mass frame , both in the longitudinal(Q_L) and transvers (Q_T) components. At very low pair opening angle θ, Q_L depends entirely on the magnitude of pion momenta (p) in the laboratory frame. At larger values of θ, an accurate measurement of Q_T relies on both θ and p resolution. Therefore resolution in p plays an essential role for atom pair detection. As a consequence of that, it needs to be known precisely in order to perform an accurate convolution of the Coulomb correlation function with experimental resolution , whenever Monte Carlo simulation is used for the analysis of pionium signal.

Because of the low Q acceptance of the experiment trigger, we cannot easily use meson resonances as calibration tools, and the best option has been to setup a simple lambda trigger. This is achieved by using an extra vertical hodoscope slab close to the beam, in order to catch the fast proton track [4].

The idea of this note is to use the analysis of lambda mass, at low opening angles, to perform a detailed quantitative assesment of momentum resolution of individual charged tracks, as function of track momentum. This resolution can be compared with the one obtained from $\pi^+\pi^-$ Monte Carlo, in order to make sure they are in perfect agreement.

Lambda mass M_Λ is determined exactly from measured decay π^- (x) and proton (y) momenta and opening angle θ, as :

$$M_\Lambda^2 = m_p^2 + m_\pi^2 + 2\sqrt{m_\pi^2 + x^2}\sqrt{m_p^2 + y^2} - 2xy\cos\theta \tag{1}$$

By squaring both sides of this equation, one realises it represents a rotated hyperbola with a physical branch in the positive quadrant of (x, y) plane :

$$m_p^2 x^2 + m_\pi^2 y^2 + x^2 y^2 sin^2\theta - \Delta^2 xycos\theta = K^2 \tag{2}$$

where $\Delta^2 = M_\Lambda^2 - m_p^2 - m_\pi^2$ and $K^2 = \left(\Delta^2/2\right)^2 - m_p^2 m_\pi^2$. For each positive value of π^- momentum x, there are two positive solutions for proton momentum y.

It is easy to show from the previous expressions that, in the low-angle approximation ($\theta^2/2 \ll 1$), the lambda mass error δM_Λ is given by:

$$M_\Lambda{}^2 (\delta M_\Lambda)^2 = \left(\frac{x}{x_0} - \frac{y}{y_0}\right)^2 \left(y_0^2 (\delta x)^2 + x_0^2 (\delta y)^2\right) \tag{3}$$

where $x_0 = \sqrt{m_\pi^2 + x^2}$ and $y_0 = \sqrt{m_p^2 + y^2}$. δx and δy are the π^- and proton momentum errors, respectively. The lowest order finite angle correction to this expression arises from a term $+x^2y^2\theta^2(\delta\theta)^2$. In order to make sure that (3) is exact to the percent level, a suitable upper cut on Q_T (actually a θ cut) must be done on lambda selection. Effectively this is achieved by $Q_T < 20MeV$, as we shall see later. As expected, formula (3) depends only on the magnitude of lab-frame momenta x and y.

Before we discuss in section 3 the analysis of single-track momentum resolution δp, we address in the next section the issue of resolution in the opening angle θ, which is the other key component for the measurement of Q_T.

2 Vertex resolution

We need a calibration tool that enables us to control the correctness of Monte Carlo description in θ resolution, with high accuracy. Although we have no source of tracks impining the detectors with "a priori" known angle, we know however that prompt $\pi^+\pi^-$ pairs are originated from a single mathematical space point inside the target intersection with the beam, in the micrometer scale.

Let us call $x_1(x_2)$ the $\pi^+(\pi^-)$ track extrapolations to the target plane in the X-coordinate, and similarly $y_1(y_2)$ for Y-coordinate. It is clear that the experimental error in the measurement of single track stereo angles (in X and Y projections) essentially determines the width of $\Delta x_v = x_1 - x_2$ and $\Delta y_v = y_1 - y_2$, which we call vertex distributions. A detailed analysis of the error propagation in the upstream arm has been carried out in earlier studies [5]. In what follows in this note, we have chosen the beam unconstraint fit for individual tracks [3]. In fact, angle resolution for prompt π^+/π^- tracks depends on the three following quantities:

- MSGC/GEM and SFD intrinsic space resolution.
- detailed material budget in upstream detector elements, including the target foil.
- lever-arm between MSGC/GEM and SFD detector planes (52.9 cm for X and 46.6 cm in Y, depending slightly on track configuration), and distance (in Z-coordinate) between middle point of the ensemble MSGC/GEM - SFD and the target (2.60 m).

Whereas the first item is essentially momentum independent, the second defines the effect of multiple scattering in upstream detector elements, and it

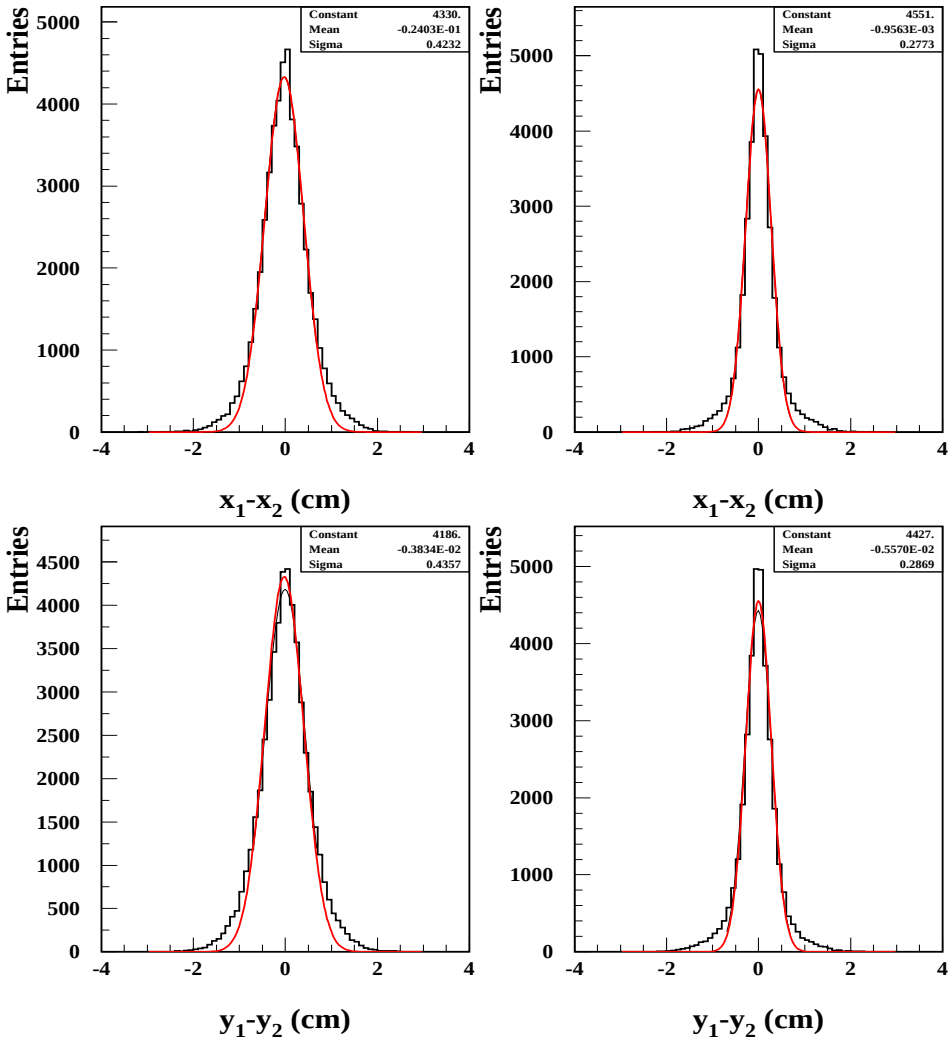

Fig. 1. *Distribution of* $\Delta x_v = x_1 - x_2$ *and* $\Delta y_v = y_1 - y_2$ *for the beam unconstrained fit, as described in the text. Slices with minimum and maximum values of average momentum were chosen as reference. Note the non-gaussian nature of the distribution tails.*

therefore scales a $1/p$ (if we neglect logarithmic corrections). The third item is known with sufficient precision.

It is important to note that, according to this reconstruction method, the error in track stereo angles (and vertex resolution) is essentially decoupled from the momentum measurement, as a consequence of having an independent upstream track. A sensitive way to test the Monte Carlo performance in θ resolution is to study the vertex distributions Δx_v and Δy_v as function of average momentum of $\pi^+\pi^-$ pair, $p = (p_1 + p_2)/2$. Histograms were fitted to a gauss function in different slices of p, and sigma values in each projection

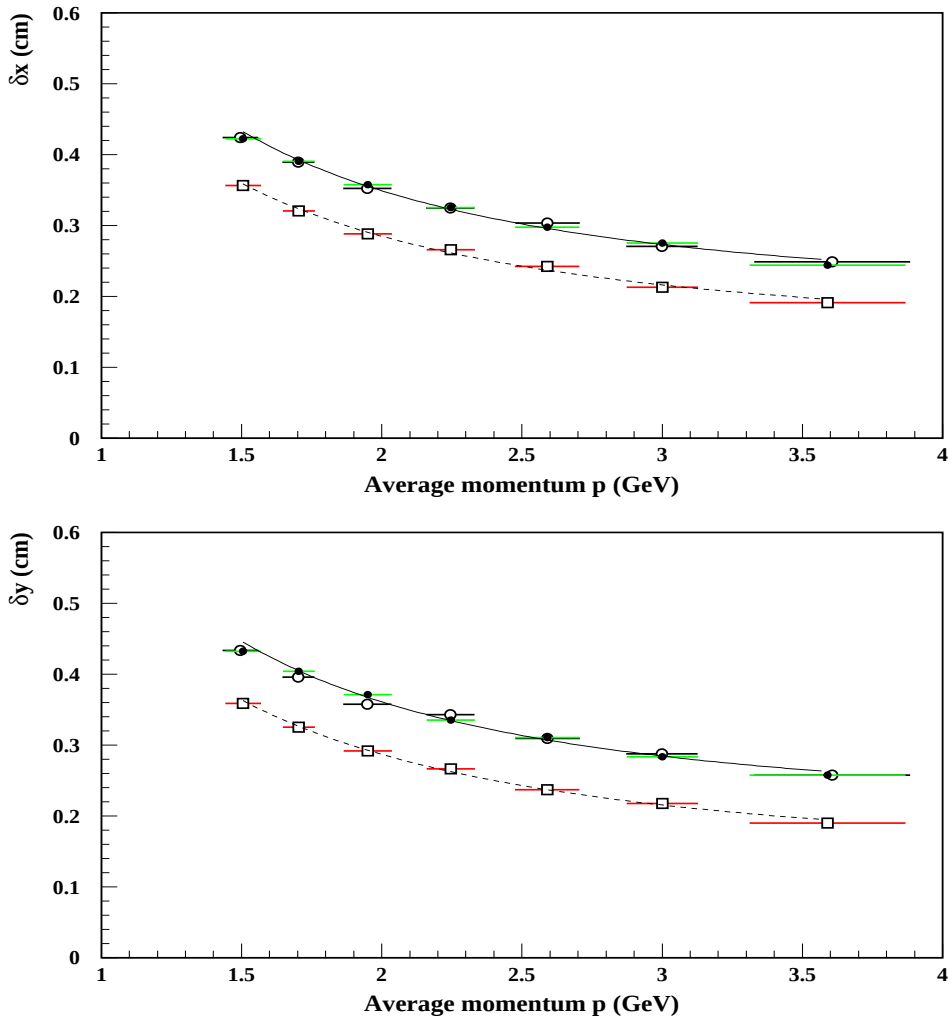

Fig. 2. *Evolution of vertex resolutions δx_v (a) and δy_v (b) (see the text), as function of average $\pi^+\pi^-$ momentum p. Black dots correspond to experimental prompt pairs, open squares to the standard Monte Carlo, and open circles to the improved Monte Carlo described in the text.*

(σ_x and σ_y) were compared with those obtained from Monte Carlo. We shall call these values δx_v and δy_v in what follows. The choice of gaussian fit does not presume a fully gaussian behaviour of the distribution tails, neither in the real data nor in Monte Carlo. It simply means an effective way to perform the comparison and its momentum scaling, since it is done consistently in both cases. In figure 1 we show the characteristics of some of these fits. In figure 2 we have plotted the evolution of fitted σ values for prompt data, as function of average momentum, for both X and Y projections. Sigma errors are given by one unit variation of the fit χ^2. We see that resolution improves for increasing p, as expected from multiple scattering.

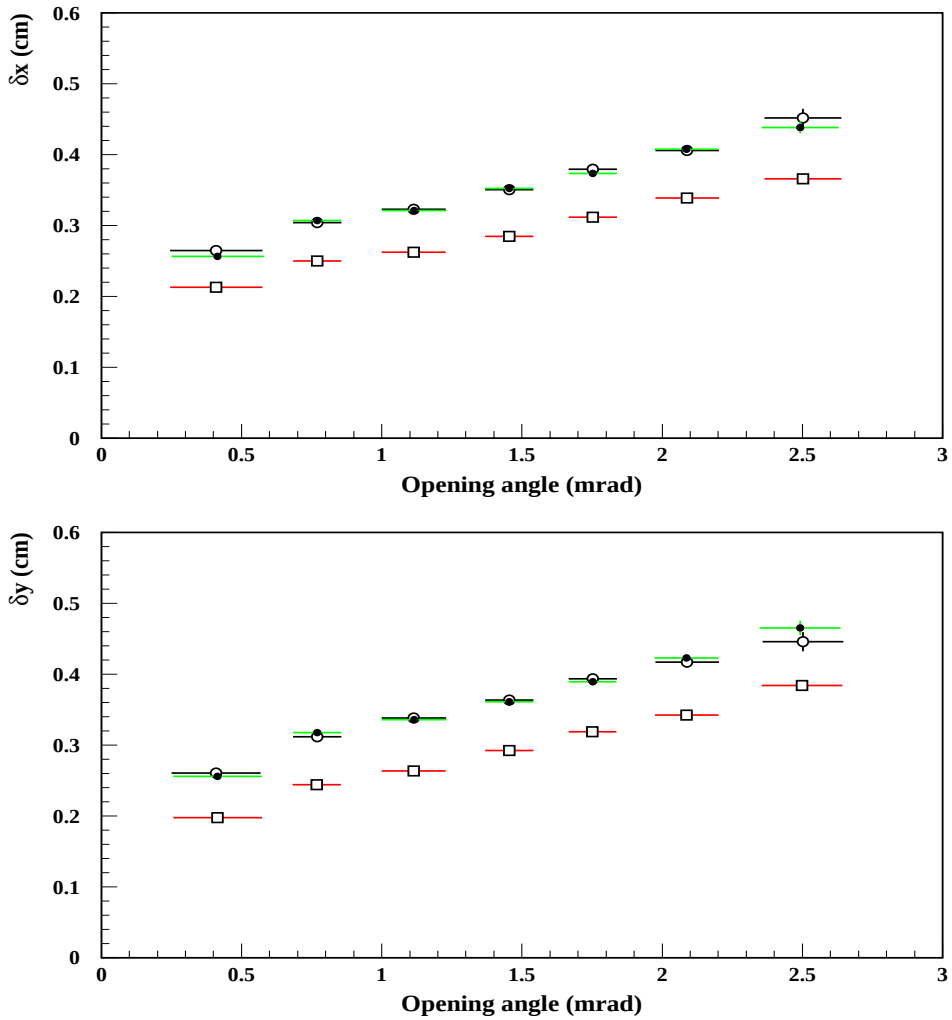

Fig. 3. *Vertex resolution δx_v (top) and δy_v (botom) as function of opening angle θ for prompt $\pi^+\pi^-$ pairs (in mrad). Note resolution improves at low angles.*

A sensible parametrisation of the vertex resolution is given by: $(\delta x_v)^2 = \alpha_x^2 + (\beta_x/p)^2$ where α_x depends on intrinsic detector resolutions in MSGC/GEM and SFD, and on the geometry factors described above. β_x in turn depends on material thicknesses and average radiation length in all upstream detector elements, including the target foil. A similar parametrisation holds for Δy_v. Clearly, whereas the α_x and α_y parameters do not have to be the same, β_x and β_y must be equal, since the same detector elements contribute in both projections. Therefore we must assume $\beta_x = \beta_y = \beta$.

By fitting expressions $(\delta x_v)^2 = \alpha_x^2 + (\beta/p)^2$ and $(\delta y_v)^2 = \alpha_y^2 + (\beta/p)^2$ to the experimental data, we can determine accurately the parameters α_x, α_y, and β. The same procedure can be applied to the Monte Carlo data. In this way,

we can make a separate tuning of detector resolutions and average multiple scattering in the Monte Carlo. The results of vertex resolution analysis for the standard Monte Carlo are represented in figure 2, along with those of real data. Also shown in this figure are the the fitted curves corresponding to the parametrisations discussed above. Parameter values obtained from the fit are given in table 1.

Table 1
Values of α_x, α_y and β parameters obtained from a simultaneous fit to the momentum dependence of vertex resolution in figure 2, using the functions $\delta {x_v}^2 = \alpha_x^2 + (\beta/p)^2$ and $\delta {y_v}^2 = \alpha_y^2 + (\beta/p)^2$. Results are indicated separately for prompt $\pi^+\pi^-$ data and different Monte Carlo options.

	α_x	α_y	β
Prompt data	0.194 ± 0.002	0.206 ± 0.002	0.576 ± 0.004
Standard MC	0.136 ± 0.002	0.138 ± 0.002	0.501 ± 0.003
Improved MC	0.196 ± 0.003	0.213 ± 0.003	0.573 ± 0.006

From the previous analysis we conclude that the standard Monte Carlo differs from real data in both average detector resolution and overall multiple scattering. Therefore we proceeded to improve the Monte Carlo in two ways: a) to degrade detector resolutions of upstream detectors by 30%, uniformely. b) to increase the overall contribution of multiple scattering by 18%. The resulting simulation will be refered to as "improved Monte Carlo" in what follows. Figure 2 shows that nearly perfect agreement is found between real data and this improved version of Monte Carlo, as far as vertex resolution is concerned.

We have also studied the behaviour of vertex resolution as function of opening angle θ, and we have compared real data with the previous Monte Carlo options. The results are shown in figure 3. Note that vertex resolution improves with decreasing values of θ, in all cases. As before, very good agreement is achieved with the improved Monte Carlo. The behaviour of δx_v and δy_v as function of θ can be understood as a consequence of the significant angle-momentum correlation present in $\pi^+\pi^-$ pairs.

3 Lambda method description

Let us now turn to the evaluation of the momentum resolution outlined in section 1. We assume that momentum error δp (for both pion and proton tracks) arises from the quadrature of two components, according to expression:

$$(\delta p)^2 = (Ap)^2 + (Bp^2)^2 \tag{4}$$

the first term, proportional to p, receives contribution from the average material thicknesses of detector elements upstream and downstream the magnet. The second term, proportional to p^2, depends on intrinsic tracking detector resolutions at both sides of the dipole (drift chambers, MSGC/GEM and SFD). The previous momentum scaling arises from the assumption that multiple scattering error scales as $1/p$, whereas intrinsic detector resolutions are assumed to be momentum independent.

Because of the kinematics of lambda decays, the negative pion acquires a momentum lower than the average $\pi^+\pi^-$ prompt tracks in DIRAC physics triggers, whereas the proton momentum is higher than this average, as it can be appreciated in figure 4. This is the ideal situation to perform a momentum analysis of the spectrometer resolution, specially if we use low angle pairs, with topology as close as possible to that of the Coulomb $\pi^+\pi^-$ pairs.

The method used is then a maximum likelihood fit to expression (3), using a sample of lambda triggers which contains not only the signal, but also the non-resonant background, due to trigger noise. The description of the latter by the likelyhood function is important if we want to have a precise determination of the A and B coefficients in (4).

For each event i, a two-dimensional likelyhood function was defined as a function of lambda mass M_i (under the $p\pi^-$ hypothesis) and the magnitude p_i of total lab-frame momentum of the pair. It reads as follows:

$$\mathcal{L}_i = \alpha \frac{P_N(p_i)}{S_N}\frac{G(M_i)}{S_G} + (1-\alpha)\frac{P_N(p_i)}{S_N}\frac{P_B(p_i,M_i)}{S_B} \tag{5}$$

where $P_N(p) = 1 + a_1 p + a_2 p^2 + \ldots$ is an Nth order polynomial in p and $G(M)$ is a gaussian function describing the resonance:

$$G(M_i) = \exp\left(-\frac{(M_i - M_\Lambda)^2}{2(\delta M_i(A,B))^2}\right)$$

where the error $\delta M_i(A,B)$ is given by expression (3) evaluated at π^- (x_i) and proton (y_i) momenta of event i. The momentum error δp is given by (4) as function of momentum, with identical A and B parameters for both particle types. The polynomial $P_B(p,M)$ describes a linear mass dependence of the background: $P_B(p,M) = 1 + b_1 M + b_2 p$. The corresponding normalisation integrals S_N,S_G and S_B must be calculated for each parameter choice, so that the likelyhood function is normalised to unity in the domain $(p_1,p_2) \times (M_1,M_2)$, where $p_{1,2}$ are the lower and upper total momentum cuts (similarly $M_{1,2}$ for the invariant mass).

The maximum likelyhood parameters are found to minimise the function:

$$-\ln \mathcal{L} = -\sum_{i=1}^{N} \ln \mathcal{L}_i(A, B, M_\Lambda, \alpha, a_k, b_l) \tag{6}$$

where N stands for the number of lambda triggers selected for the fit, and $\mathcal{L}_i$ is the likelyhood function evaluated for event i characterised by measured values x_i,y_i,M_i and p_i.

The overall likelyhood $\mathcal{L}$ for N lambda events significantly increases when each measured proton momentum y_i is replaced, in expression (3) for δM_i, by one of the hyperbolic solutions of equation (2), corresponding to the measured π^- momentum x_i. This is equivalent to take advantage of the lambda mass constraint in momentum scaling of δp (4), together with the fact that π^- momentum has allways the smallest error.

A straightforward procedure is to determine first the a_k and b_l coefficients of the polynomials, by performing a fit to the background only. Once these parameters are fixed, M_Λ,α,A and B can be left free in the final fit. All minimisations were performed by MINUIT program [1].

4 Selection of lambda events

We have applied the analysis described in the previous section to the DIRAC 2001 Ni target data sample, because these data have been chosen by the collaboration for a first determination of pionium production and lifetime. Lambda triggers are routinely taken at constant fraction of total spill rate during normal physics runs, and they have been subject to the standard calibrations for 2001 data periods. Reconstruction was done with ARIANE program [2], using the full tracking procedure option [3].

The upstream track pattern recognition was run with the standard parameters used for $\pi^+\pi^-$ prompt pair selection, which implies that only tracks pointing to the beam intersection with the target plane within 3 σ will be reconstructed, σ being track resolution in the transvers (XY) plane. No attempt has been made to enlarge these pattern recognition windows in the present analysis. Admittedly, this causes a bias in lambda selection which has the general trend to enhance the signal at short decay path. We have prefered this option in order to keep the tracking performance as close as possible to that with $\pi^+\pi^-$ pairs, which we want to evaluate.

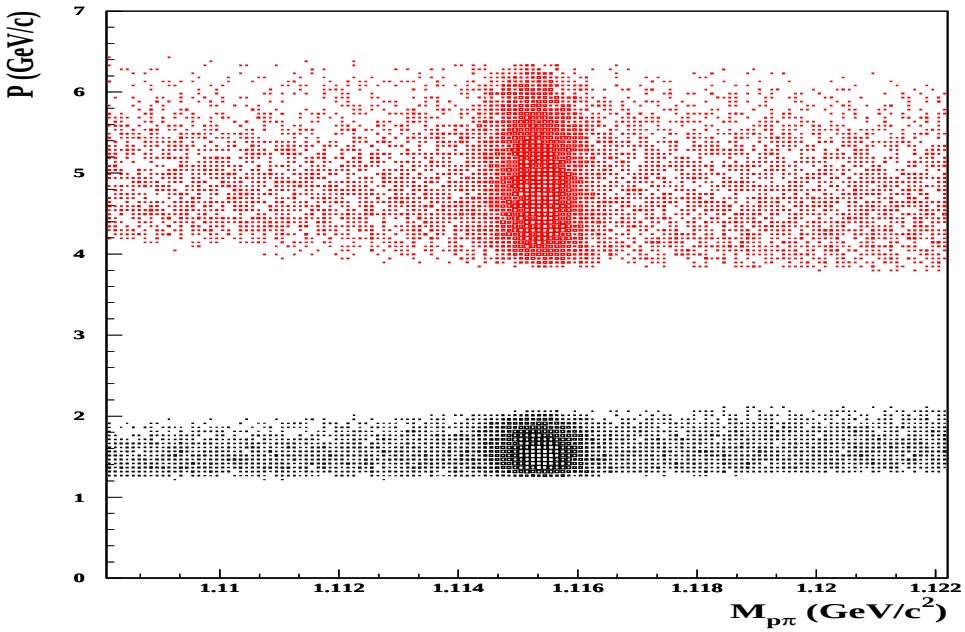

Fig. 4. *Scatter plot representing the measured invariant mass (under $p\pi^-$ hypothesis) versus positive (red colour) and negative (blue colour) track momenta, for lambda triggers of 2001 run. A clear momentum gap can be appreciated, due to lambda decay kinematics and vertical hodoscope time cuts.*

Time difference $t_2 - t_1$ between positive and negative tracks in vertical hodoscope TDCs is restricted to the interval $0 < t_2 - t_1 < 1.3\ ns$. A decay vertex is determined by finding the point of closest approach between both tracks, and the probability of track intersection at that particular point (P_v) is then calculated. Also a joint track probability is defined as the one corresponding to $\chi^2 = \chi^2_1 + \chi^2_2$, where $\chi^2_{1,2}$ are the fit χ^2 for each individual track. Both P_v and P_t are required to be larger than 1%. The invariant mass is calculated according to expression 1, taking into account the parallax error in θ due to displaced vertex.

In figure 4 we see a scatter plot of individual track momenta (π^- and proton) versus reconstructed invariant mass, showing the momentum range covered by this analysis. The mass projection from previous plot is better appreciated in figure 5, showing average mass resolution of $0.39 MeV/c^2$.

In figure 6 selected lambda events are mapped onto the (Q_L,Q_T) plane. As expected, they lie on a circular coronna whose width is determined by our mass resolution. It can be appreciated that a cut $Q_T < 20 MeV$ is enough to ensure that mass resolution is determined by Q_L resolution only, and therefore relation (3) is fulfilled. In figure 7 we show the lambda momentum and opening angle distributions.

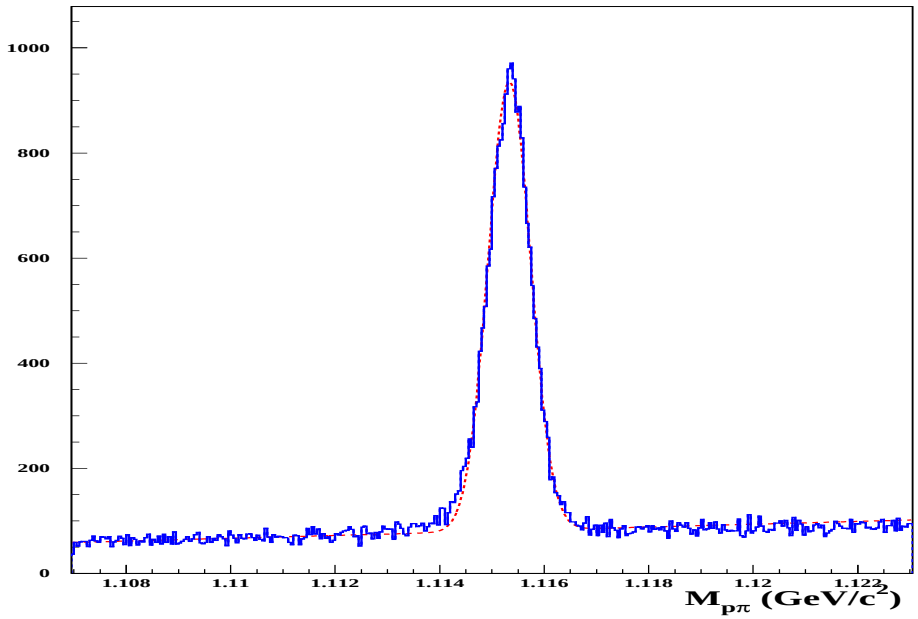

Fig. 5. *Invariant mass spectrum obtained from the projection of scatter plot in figure 4. A gaussian fit with linear background is also shown for reference, with* $\sigma = 0.39 MeV/c^2$, *and* $M_{p\pi} = 1115.4 MeV/c^2$.

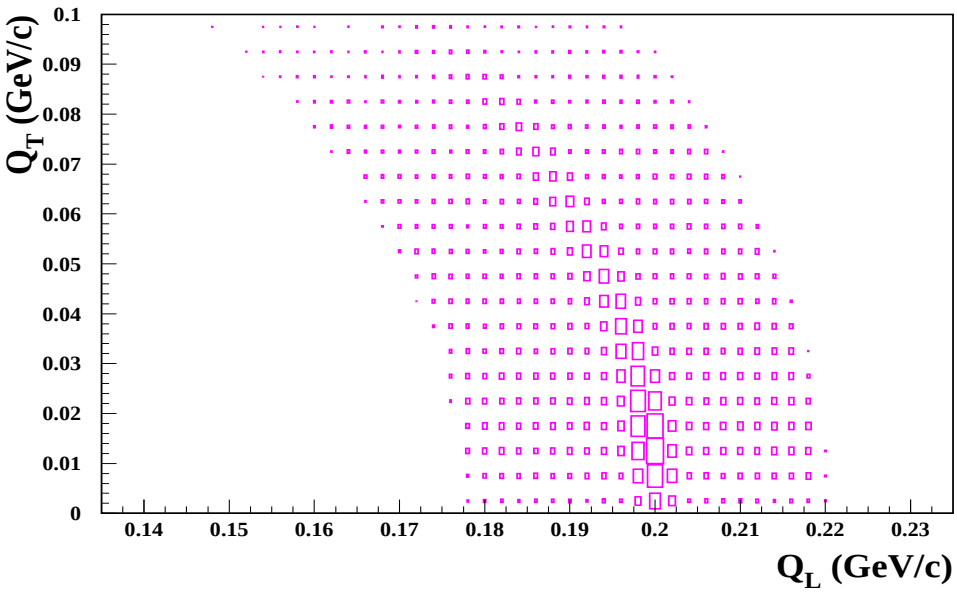

Fig. 6. *Longitudinal* (Q_L) *versus transvers* (Q_T) *momentum in the lambda center-of-mass frame, with respect to its direction of flight. Lorentz transformation is done under* $p\pi^-$ *hypothesis. A mass cut* $1.1140 < m(p\pi^-) < 1.1165$ *has been applied.*

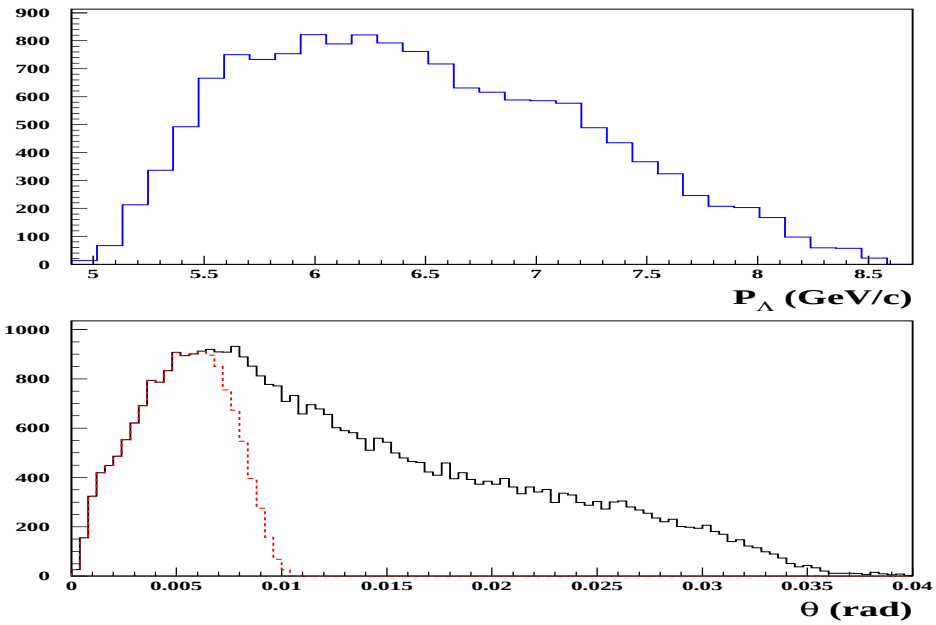

Fig. 7. *For lambda events defined by the mass cut used in figure 4, (a) shows the magnitude of vector sum of proton and π^- momenta for lambda events, and (b) the opening angle θ between the two tracks. The dotted red line shows the effect of the $Q_T > 20 MeV/c$ cut.*

Table 2
Parameters obtained for the maximum likelyhood fit to the experimental lambda sample of 2001, as defined in the text. Quoted errors correspond to variation of 0.5 units of the likelyhood function.

A	$(0.277 \pm 0.003) \times 10^{-2}$
B	$0.205^{+0.033}_{-0.038} \times 10^{-3}\ GeV^{-1}$
M_Λ	$1115.410 \pm 0.005\ MeV/c^2$
α	0.529 ± 0.005
b_1	12.8 ± 1.9
b_2	-0.047 ± 0.009

a_1	-66.014 ± 0.048
a_2	36.205 ± 0.007
a_3	-7.3399 ± 0.0009
a_4	0.65470 ± 0.00002
a_5	-0.02176 ± 0.00001

5 Results and comparison with Monte Carlo

The fit procedure described in section 2 was applied for Ni 2001 data, and table 2 gives the maximum likelyhood parameters found. Errors are given by variation of $-ln\mathcal{L}$ by 0.5 units, on positive and negative side of the minimum. We can summarise the result by plotting the relative momentum error $\delta p/p$ as function of momentum, according to the expression $\delta p/p = \sqrt{A^2 + B^2 p^2}$, with

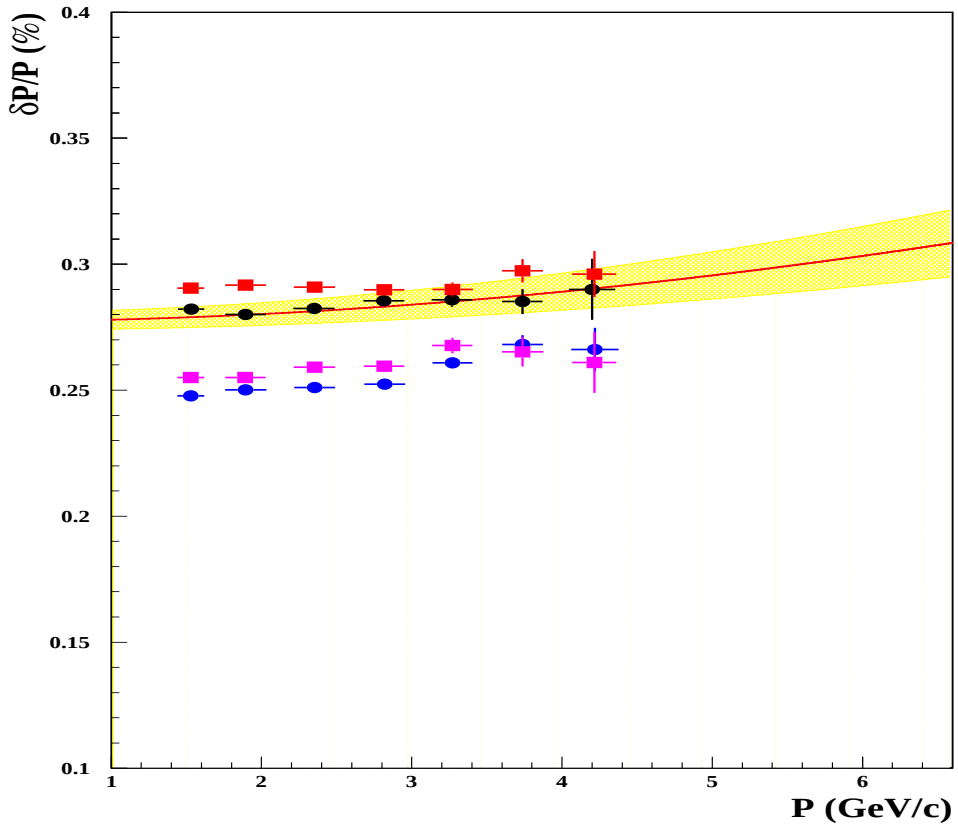

Fig. 8. *Relative momentum error $\delta p/p$ as function of track momentum. The red continuous line represents the parametrisation $\sqrt{A^2 + B^2 p^2}$ as determined from the measured values of A and B after maximum likelyhood fit to experimental lambda data. The yelow band represents $\pm 1\sigma$ variation of the parameters. Blue dots indicate resolution of standard $\pi^+\pi^-$ Monte Carlo, according to input generator information. Purple squares correspond to improved Monte Carlo after upstream detector elements give a perfect fit, according to the analysis in section 2. Black dots correspond to a further improved Monte Carlo where the average multiple scattering in downstream detectors has been increased by 10%. Red rectangles show the same option as before for upstream arm, but 18% multiple scaterring increase downstream.*

A and B as determined by the fit. This is shown by the red line in figure 8, where a yellow coloured band represents the $\pm 1\sigma$ error variation taken simultaneously in both parameters. The fact that $\delta p/p$ is found to be nearly constant indicates that spectrometer resolution is dominated by multiple scattering, rather than by intrinsic detector resolution. At $p = 2.5 GeV/c$, the relative momentum error is 0.281 % , for the overall 2001 datataking period analysed. The B parameter is small , $2.0^{+0.3}_{-0.4} \times 10^{-4} GeV^{-1}$, but significantly away from zero. Introduction of the finite angle correction term $+x^2 y^2 \theta^2 (\delta\theta)^2$ (see section 1) with $\delta\theta = 5 \times 10^{-4}$ estimated from Monte Carlo, resulted in a negligible change in the previous parameter values and likelyhood function.

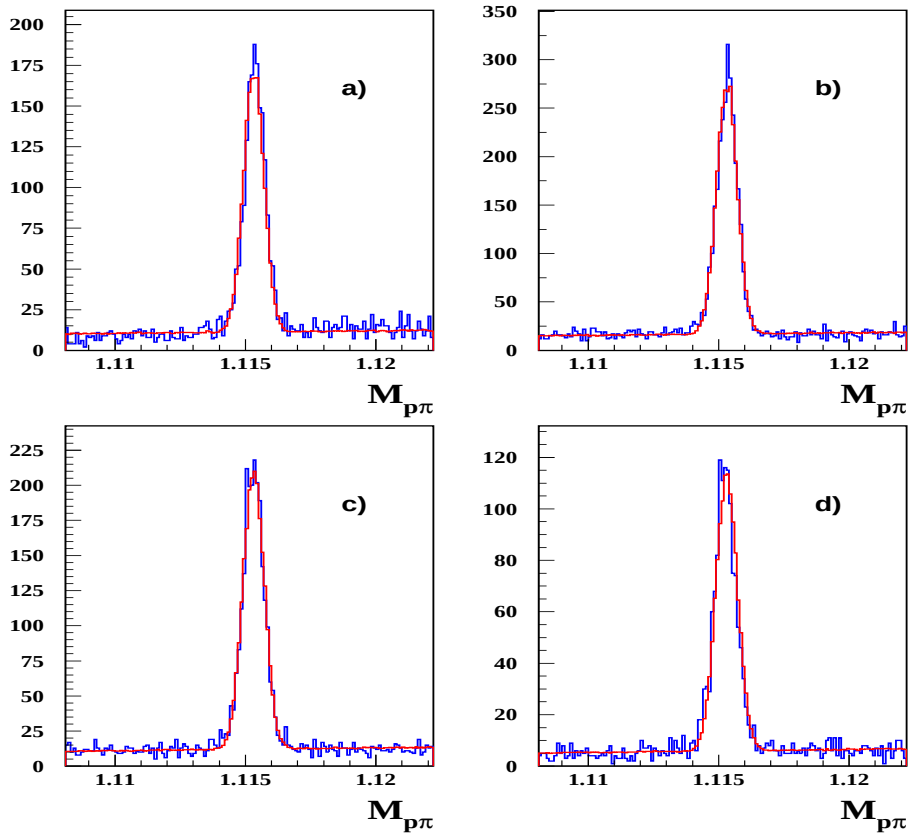

Fig. 9. *Visualisation of maximum likekyhood fit quality. Invariant mass spectra are shown in four slices of lambda momentum, namely a)* $5 < p(GeV) < 5.75$, *b)* $5.75 < p(GeV) < 6.5$, *c)* $6.5 < p(GeV) < 7.25$, *d)* $7.25 < p(GeV) < 8$. *The fit results, with parameters given in table 2, are indicated by the red coloured line.*

The fit results can be visualised using a weighing procedure according to the $\mathcal{L}$ function at maximum, applied to random values in the domain $(p_1, p_2) \times (M_1, M_2)$. This is represented in figure 9, where the mass spectrum is shown in four slices of lambda momentum, with a superimposed coloured line representing the fit results. Note the fit parameters are unique, in particular the mass, as given by table 2. The fit projection onto the p spectrum is shown in figure 10. The fit quality appears to be good in both projections.

Now we can compare the previous results with Monte Carlo data [6], [8]. In Monte Carlo, the original track momentum p_g [7] is of course known "a priori" from the generator, therefore by performing the full ARIANE reconstruction we can determine $\delta p/p$ as function of p for individual tracks. This is done by means of a gaussian fit to the distribution of observed differences of inverse

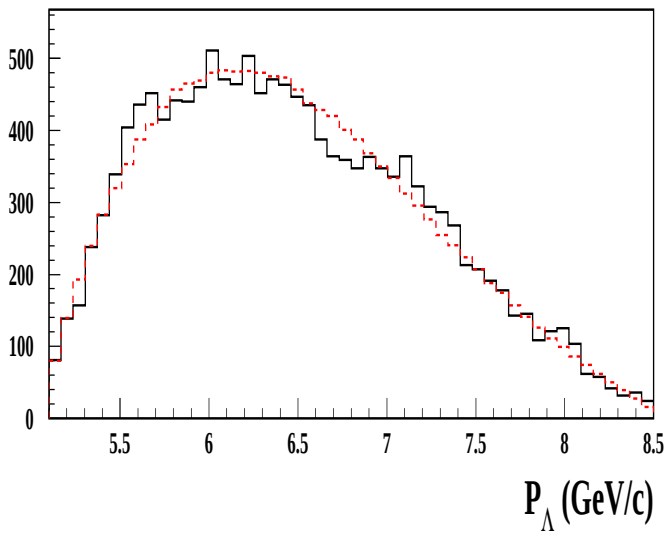

Fig. 10. *Visualisation of maximum likekyhood fit quality, projected into the spectrum of total momentum p. Coloured line is constructed according to parameters in table 2.*

momenta $1/p - 1/p_g$. There are two possibilities open, as far as the generator is concerned:

- to use a lambda production Monte Carlo
- a standard $\pi^+\pi^-$ generator with Coulomb correlated pairs

Within the first case, we still have two different ways to determine momentum resolution, namely:

a) to proceed as explained before, using knowledge of original track momentum
b) to treat the lambda Monte Carlo data as if they were real events, and apply to them the maximum likelyhood analysis described in section 2. Null background ($\alpha = 1$) should be assumed in this case.

A detailed comparison between methods a) and b) above provides an important consistency check for the low decay angle method described in section 2, and approximation made in section 1. The results should coincide. A confirmation that this indeed happens is given in figure 11.

Now a comparison between the resolution obtained with $\pi^+\pi^-$ Monte Carlo and the one from lambda method (b) above) tells us whether the hypothesis that the proton in lambda decay behaves like a pion with identical momentum is a good approximation or not, in terms of momentum resolution. The results

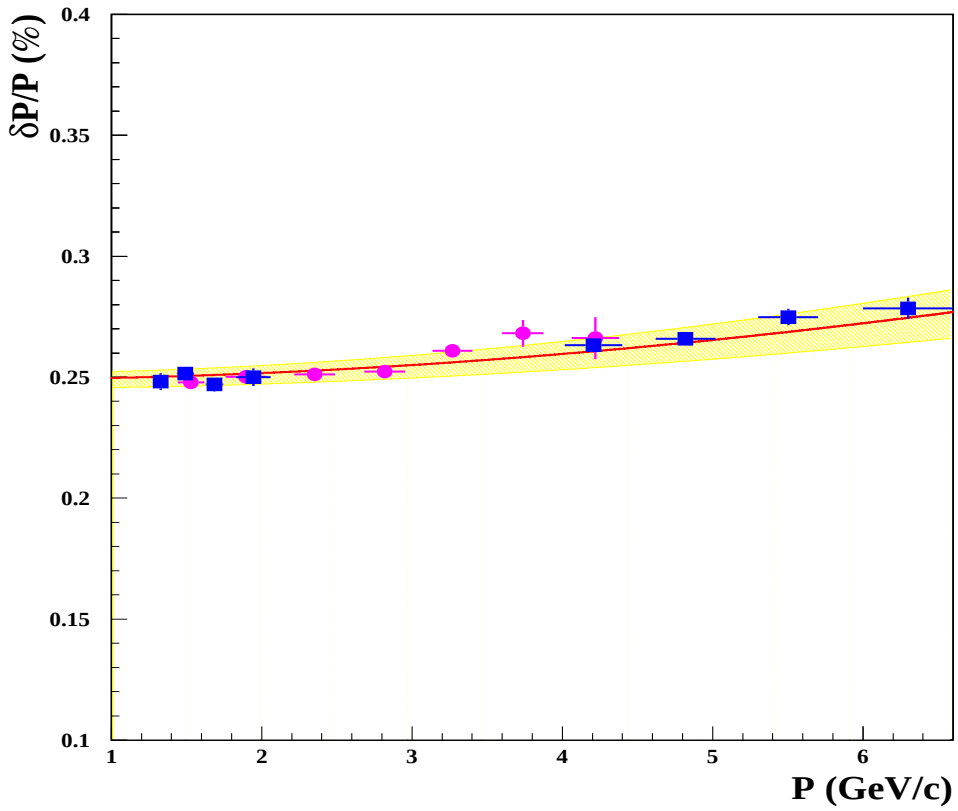

Fig. 11. *Relative momentum error $\delta p/p$ as function of track momentum. The red continuous line represents the parametrisation $\sqrt{A^2 + B^2 p^2}$, with A and B determined from a maximum likelyhood fit to lambda Monte Carlo, following the same procedure as in figure 8 with real data. Lambda Monte Carlo has default values of materials file and detector resolutions. The yellow band represents $\pm 1\sigma$ simultaneous variation of the parameters. Blue squares indicate resolution of the same Monte Carlo, but determined directly from the generator input information. Purple dots indicate resolution of standard $\pi^+\pi^-$ Monte Carlo.*

from $\pi^+\pi^-$ have been overlayed to the lambda decay ones in figure 11 with purple coloured dots. We can see that they are well compatible, within errors.

Needless to say that all of the above comparisons require the Monte Carlo simulations to be performed at exactly the same conditions of material thicknesses and detector resolutions, in order to make sense. The standard materials file was used in all cases, with default detector resolution parameters, as refered to in section 4.

Once the previous cross-checks have been made, we can turn back to the main objective, namely to find out whether the momentum resolution in the $\pi^+\pi^-$ Coulomb correlated Monte Carlo is correctly described or not. In other words, we want to determine accurately what changes need to be made to the

standard Monte Carlo in order to achieve a perfect description of momentum resolution, and at the same time of vertex resolution, according to the discussion made in section 4. Only then we can fully trust the Monte Carlo as normalisation reference for the Coulomb pair background, in our search for pionium breakup signal.

In figure 8 we show again the curve of $\delta p/p$ determined from the data (red line), along with the resolution obtained from $\pi^+\pi^-$ Monte Carlo for three different options, namely: a) the standard version with default values of material budget and detector resolution parameters (blue). b) the improved version described in section 4 (purple). c) the upstream part as before, but downstream multiple scattering increased by 10% (black), with standard drift chamber resolution.

6 Conclusions

DIRAC spectrometer, by means of its upstream detector arm, provides a precise and reliable instrument for analysis of pionium breakup signal. Both momentum and opening angle resolution are analysed in detail in this note using experimental data from 2001 run. These results are used to constrain sensitive parameters of the Monte Carlo simulation, like material budget and intrinsic detector resolutions, separately for upstream and downstream arms. A final Monte Carlo simulation is found which exactly matches the experimental data. Momentum resolution in DIRAC is found to be accurately described by a parametrisation $(\delta p/p)^2 = A^2 + B^2 p^2$ with $A = 0.277 \pm 0.003$ % and $B = (2.0^{+0.3}_{-0.4}) \times 10^{-4} GeV^{-1}$.

7 Acknowledgements

We specially thank Panos Kokkas for having made available to us lambda trigger files for 2001, and Monte Carlo output. Discussion with him concerning lambda selection and resolution was particularly useful. Cibrán Santamarina and Christian Schuetz helped us clarify a number of aspects of Monte Carlo production. Finally, Juan José Saborido and Manuel Sánchez provided us the invaluable help of allowing our reconstruction jobs into their GRID cluster at CESGA, during specific gaps of LHCb production.

References

[1] MINUIT, Function Minimization and Error Analysis. Reference Manual. Version 94.1. F. James.
MINUIT, version 94.1, http://wwwasdoc.web.cern.ch/wwwasdoc/minuit.minmain.html

[2] The DIRAC offline User Guide. Daniel Drijard, Michel Hansroul and Valery Yazkov.

[3] NOTE 03-08: A Tracking System for Upstream Detectors in DIRAC. B. Adeva, A. Romero and O. Vázquez Doce.

[4] B. Adeva et al. DIRAC : A High Resolution Spectrometer for Pionium Detection . NIM Nucl. Instr. Meth. A515 (2003) 467-496.
L. Afanasev, The multilevel trigger system of the DIRAC experiment, hep-ex/0202045, Nuc. Instr. and Meth. A 491 (2002) 376.

[5] DIRAC note 00-07. Uncertainties induced by multiple scattering in upstream detectors of the DIRAC setup . M. Pentia and S. Constantinescu. (Part I: Vertex Position Uncertainty)
DIRAC note 01-04. Uncertainties induced by multiple scattering in upstream detectors of the DIRAC setup . M. Pentia and S. Constantinescu. (Part II: Relative Momentum Resolution)

[6] NOTE 98-08. The GEANT-DIRAC Simulation Program Version 2.5. P. Zrelov and V. Yazkov.
http://zrelov.home.cern.ch/zrelov/dirac/montecarlo/instruction/instruct26.html

[7] DIRAC note 04-02: DIRAC events generator, C. Santamarina.

[8] DIRAC Note 2004-04: Summary on Λ decay analysis for Ni 2001 to 2003. Panagiotis Kokkas.